Antimony composition impact on band alignment in InAs/GaAsSb quantum dots

I. Saïdi, K. Boujdaria, C. Testelin

Antimony composition impact on band alignment in InAs/GaAsSb quantum dots

I. Saïdi[1],* K. Boujdaria[1], and C. Testelin[2]

[1] *Université de Carthage, Faculté des Sciences de Bizerte, LR01ES15, Laboratoire de Physique des Matériaux: Structure et Propriétés, 7021 Zarzouna, Bizerte, Tunisia*

[2] *Sorbonne Université, CNRS-UMR 7588, Institut des NanoSciences de Paris, F- 75005 Paris, France.*

(Dated: July 18, 2024)

Abstract

We present a theoretical study of the electronic and excitonic states in InAs/GaAsSb quantum dots. We first center our study on the dependence of the antimony composition in the positioning of conduction- and valence- band alignments in InAs/GaAsSb/GaAs heterostructures. We predict a transition from type I to type II quantum dots at critical composition $x_c = 0.128$, which describes well the experimental trend. We discuss the influence of the quantum dot size and antimony composition on the spatial distributions of carriers and the exciton binding energy. We find that the ground state exciton binding energy is always significantly smaller ($\simeq 4\,\text{meV}$) for type II than for corresponding type I quantum dots ($\simeq 14\,\text{meV}$). Finally, we also predict the excitonic radiative lifetime and find 1 ns for type I and 10 ns for type II quantum dots, in agreement with the existing experimental literature.

PACS numbers:

*Electronic address: imen.saidimokded@fsb.ucar.tn

I. INTRODUCTION

Quantum dots (QDs) with a type II band line-up have been the object of intensive research due to their potential applications in different domain as the quantum technology and optoelectronic field. Separating electron or hole outside the nanostructure makes type II QD a good candidate to realize the QDs memories [1, 2], QD solar cells in near-infrared spectral range [3] and optoelectronic devices including lasers [4]. In parallel, several studies have been carried out in order to realize the intermediate band solar cell structures (IBSCs). The IBSC was suggested to increase the performance of existing solar cell technologies by using several types of QD/matrix system [5–9]. In this context, the InAs/$GaAs_{1-x}Sb_x$ QDs are one of promising candidate to elaborate the IBSC since the use of GaAsSb as a buffer layers enhances the QDs properties leading to uniform and isotropic nanostructure [10]. Controlling the Sb composition in the type II InAs/GaAsSb QDs is another crucial factor to elaborate highly tunable and emissive IBSC.

In type II InAs/GaAsSb QDs, the electron is confined inside the InAs dot hence acting as the barriers for the hole which remains in the layers GaAsSb. Comprehending the electronic properties of semiconductor (SC) alloys is a crucial step in modeling and engineering devices. It is also essential for understanding the physics underlying such heterostructures. Few studies were focused on the crossover from type I to type II band line-up of InAs QDs by varying the Sb composition in the $GaAs_{1-x}Sb_x$ matri while theoretical investigations are still required. Evidence of type I-type II transition have been observed in InAs/$GaAs_{1-x}Sb_x$ QDs. The critical composition is not well established, even though it serves as a key tool for optimizing InAs/GaAsSb quantum dots (QDs) to make them more suitable for photovoltaic applications. Theoretical calculations [11] predict a type II band alignment when the Sb composition exceeds $\sim 12\%$ which can be compared to other reported experimental values [10, 12, 13]. Experimental evidences for a type I-type II transition, occurred at $x = 13\%$, have been obtained by using precise optical tools such as power-dependent photoluminescence (PL) and time-resolved photoluminescence (TRPL) measurements. Once again, experimental results [14] have also supported this assertion by showing a significant decrease of the carrier lifetime highlighting the modification from type I to type II band alignment. Moreover, while other studies predicted such transition occurs between 10% and 14% [16, 17], in parallel Ban *et al* [18] reported that the passage from type I to type II

band line-up occurs for an Sb composition ranging from 13% to 15%. For the sake of simplicity, many publications employ linear interpolations or extrapolations. Nevertheless, this procedure is too coarse to produce satisfactory results and is at times not recommended. Consequently, high-quality predictions of the band parameters of these alloys is required due to their significant dependence on the alloying composition parameter x. Furthermore, any dependable theoretical computation to the electronic properties of the heterostructure necessitates a realistic description of the strained bulk SC.

In this paper, we propose to investigate the band alignment transition from type I-type II in InAs QDs in view of strain effects as well as antimony composition in $GaAs_{1-x}Sb_x$ matrix. In the framework of the effective mass approximation, we calculated the electron and hole energy levels, and binding energy while taking into account the Coulomb interaction.

In the present theoretical approach to excitonic structure, the full configuration interaction (CI) is not considered for excitons; in type I, the excited states are highly energetic, and in type II, electrons and holes are localized in different areas, reducing overlap and Coulomb coupling. Both effects significantly reduce the CI contribution. As a result, we have limited our calculations to the direct electron-hole Coulomb interaction.

The paper is organized as follows. In Section 2, we will discuss the influence of Sb composition on the band line-up of the InAs/GaAsSb/GaAs heterostructure, and thereby deduce an accurate and adapted band parameters useful for InAs/GaAsSb QDs modelization. Section 3 is divided in two parts. In part 3.1, we will describe our theoretical model which includes the QD shape modelling and the calculation of the excitonic transition energy and the radiative exciton lifetime. The predicted results are presented in part 3.2 and we will compare PL and TRPL experimental data to theoretical predictions. Finally, conclusions are given in section 4.

II. BAND PARAMETERS IN STRAINED CONSTITUENT MATERIALS

A. Calculation procedure

We propose to calculate the $InAs/GaAs_{1-x}Sb_x/GaAs$ band line-up by using the total Hamiltonian $\mathcal{H} = \mathcal{H}_{\mathbf{k.p}} + \mathcal{H}_S$, where $\mathcal{H}_{\mathbf{k.p}}$ is the 40-band **k.p** Hamiltonian [19, 20] and $\mathcal{H}_S$ is the strain Bir-Pikus Hamiltonian [21]. The 40-band **k.p** formalism was introduced by

following the approach described in Refs. [20], while incorporating the widely recognized Bir-Pikus correction for strained. The comprehension of accommodating lattice mismatch strain effect becomes crucial when attempting to realize QDs with a substantial number of layers in a barrier matrix. Bremner et *al* experimentaly investigated the stress relaxation on an ensemble of InAs/GaSbAs QDs [22]. Results from transmission electron microscopy and X-ray diffraction indicate that the onset of relaxation in the GaAsSb layers occurs when the Sb content is approximately 15%. Therefore, we are considering the interface InAs/GaAs for contents below 15% due to the fact that the relaxation in GaAsSb layers is zero. In the following, we have considered two interfaces, namely GaAsSb/GaAs and InAs/GaAs, denoted by (1) and (2), respectively. The superscript U(S) means the unstrained (strained) case.

Using the potential theory's formalism [23], the strain-induced shifts for CB and VB are given by:

$$\delta E_C = a_c \epsilon_H = 2a_c \left(1 - \frac{C_{12}}{C_{11}}\right) \epsilon_{\parallel} \tag{1}$$

$$\delta E_{HH} = a_v \epsilon_H - b_v \epsilon_B = -\left(P_\epsilon + Q_\epsilon\right) \tag{2}$$

$$\delta E_{LH} \;=\; -P_\epsilon + \tfrac{1}{2}\left(Q_\epsilon - \Delta + \sqrt{\Delta^2 + 2\Delta Q_\epsilon + 9Q_\epsilon^2}\right) \tag{3}$$

where Δ denoted the spin-orbit coupling, $\Delta = \left|E_{\Gamma_8} - E_{\Gamma_7}\right|$. P_ϵ and Q_ϵ are defined as:

$$P_\epsilon = -2a_v \left(1 - \frac{C_{12}}{C_{11}}\right) \epsilon_{\parallel} \tag{4}$$

and

$$Q_\epsilon = -b_v \left(1 + 2\frac{C_{12}}{C_{11}}\right) \epsilon_{\parallel}$$

In these expressions a_c and a_v represent the hydrostatic deformation potential for the CB and VB, respectively, and b_v is the shear deformation potential. C_{11} and C_{12} are the elastic stiffness constants. $\epsilon_H = \epsilon_{xx} + \epsilon_{yy} + \epsilon_{zz}$ and $\epsilon_B = \epsilon_\perp - \epsilon_\parallel$ denote the hydrostatic and biaxial strain, respectively. The in-plane strain is calculated directly following the basic relationship:

$$\epsilon_\parallel = \epsilon_{xx} = \epsilon_{yy} = \frac{a_0 - a}{a}$$

where a_0 and a are the lattice constants of the barrier material and the strained material, respectively. Along the growth direction, the strain can be expressed as:

$$\epsilon_{\perp} = \epsilon_{zz} = -2\frac{C_{12}}{C_{11}}\epsilon_{xx}$$

Taking into account the strain effects, the confinement potentials for an electron and a heavy-hole (HH) are given by:

$$\Delta E_C^{(\alpha),(S)} = \Delta E_C^{(\alpha),(U)} + \delta E_C^{(\alpha)} \qquad (\alpha = 1 \text{ or } 2) \tag{5}$$

$$\Delta E_V^{(\alpha),(S)} = \Delta E_V^{(\alpha),(U)} + \delta E_{HH}^{(\alpha)} \tag{6}$$

in which:

$$\Delta E_\beta^{(1),(U)} = Q_\beta^{(1)}(E_g(GaAsSb) - E_g(GaAs)) \qquad (\beta = C \text{ or } V) \tag{7}$$

$$\Delta E_\beta^{(2),(U)} = Q_\beta^{(2)}(E_g(InAs) - E_g(GaAs)) \tag{8}$$

where Q_C and $Q_V = (1 - Q_C)$ are CB and VB offset constant, respectively.

As quoted in Ref. [24], there is no clear consensus on the type of the band alignment in GAsSb/GaAs system. The CB and VB offsets depend not only on the materials constituting the nanostructure but also on the impact of the lattice-mismatch at the interface. Table I summarizes the numerical parameters used to calculate the band line-up.

	GaAs	GaSb	InAs
a ($\mathring{A}$)	5.65+3.88 $10^{-5}(T-300)$	6.09+4.72 $10^{-5}(T-300)$	6.06+2.74 $10^{-5}(T-300)$
E_g (eV)	1.52	0.81	0.42
a_c (eV)	-7.17	-7.50	-5.08
a_v (eV)	1.16	0.80	1
b_v (eV)	-2.00	-2.00	-1.80
C_{11} (MPa)	1.22	0.88	0.83
C_{12} (MPa)	0.57	0.40	0.45

TABLE I: *The band parameters of constituent materials used to calculate the conduction-band and valence-band offsets. The band parameters are taken from Ref. [25].*

The bandgap of unstrained $GaAs_{1-x}Sb_x$ alloy (E_g^U) has a quadratic dependence on Sb composition. One commonly uses the following empirical expression at $T = 300\,\mathrm{K}$ provided by Ref .[26].

$$E_g^U\,(eV) = 1.519 - 1.909x + 1.2x^2$$

Several earlier works [27, 28] have reported contradictory results on the GaAsSb/GaAs type-II band alignment mainly due to the wide range of values for VB offsets constant $Q_V^{(1)}$ used in the literature. In particular, Ji et *al* [29] and Peter [30] have pointed large values, ranging from 1.7 to 2.1, while, Prins et *al* [26] have predicted a weak band alignment using $Q_V^{(1)} < 1$. The overestimation of high $Q_V^{(1)}$ values can be attributed to the excessive appraisal of both the unstrained band gap and hydrostatic deformation potential. Indeed, the scatter in Q_V obtained is closely dependent on the exact determination of E_g. Therefore, a value of Q_V, approximately 0.90 [31], would be needed to obtain a good agreement between the computed transition energies and most of the experimentally measured values in the literature [32, 33]. This value is marginally lower than the experimental value reported in Ref [27], which suggests $Q_V^{(1)} = 1.05$.

B. Band alignment transition

Fig. 1(a) schematically illustrates the CB offset (δE_C) and the VB offsets ($\delta E_{HH}, \delta E_{LH}$) (HH, LH denote the heavy-hole and the light-hole, respectively) for the $GaAs_{1-x}Sb_x$/GaAs heterostructures as a function of the Sb composition. Clearly, we can deduce the energy E_g^ℓ ($\ell = U$ or S)decreases when the Sb composition, x, increases. However, all other quantities $\delta E_C, \delta E_{HH}$ and δE_{LH} increase with increasing Sb composition. In Fig. 1(b), the band alignments for the InAs/GaAs system is shown for both cases, InAs strained and unstrained. The band offset of hole has been taken $\Delta E_V^{(2),(U)} = 85\,\mathrm{meV}$ as given in Ref [34]. Descriptions of such band offset are widely scattered throughout the literature, while only some of them which predicted a common values [35]. The strain is taken into account in our calculation via the hydrostatic and the biaxial components ($\epsilon_H = 7.7\%, \epsilon_B = 12.3\%$) as outlined by Lazarenkova et *al* [36]. They considered inclusion of the anharmonicity in strained InAs/GaAs systems results in a less intense compressive hydrostatic compared to the commonly employed quasiharmonic approximation. This leads to an enhance-

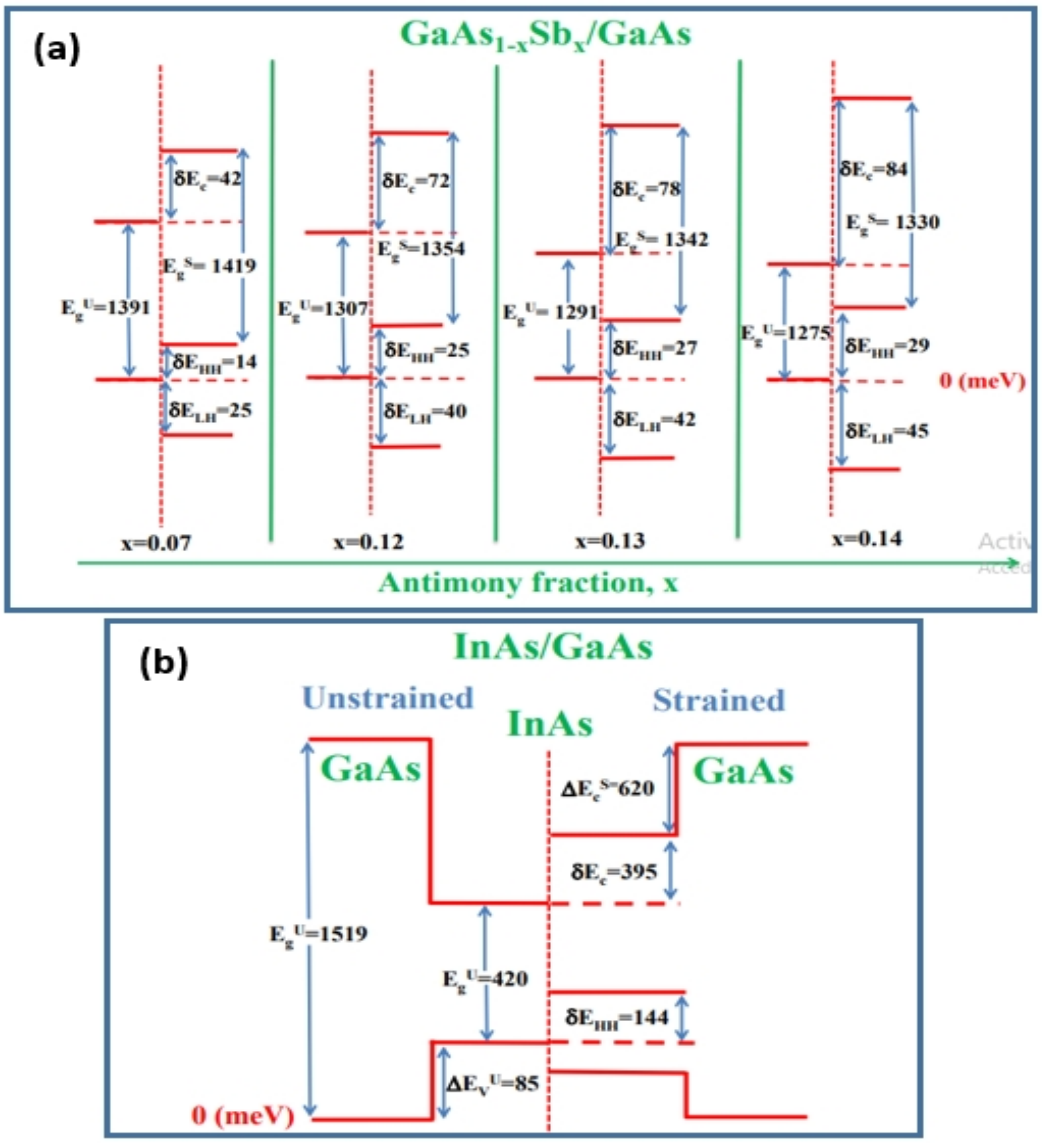

FIG. 1: *(a)* Evolution of *conduction- and valence-band alignments as a function of Sb composition, for* $GaAs_{1-x}Sb_x/GaAs$ *heterostructure. (b)* Estimated *conduction- and valence- band alignments deduced from our calculations for InAs/GaAs heterostructure. A*ll energies are given in meV.

ment in the agreement between the computed electron band offset and experimental values. Thus, the band edges of CB and VB obtained under the considered strain effect are $\delta E_C^{(2)} = 395\,\text{meV}$ and $\delta E_{HH}^{(2)} = 144\,\text{meV}$, respectively. We can deduce the corresponding CB offset $\Delta E_C^{(2),(S)} = 620\,\text{meV}$, which is in good agreement with published values given in Refs [37, 38], where the authors predict a value around 690 meV.

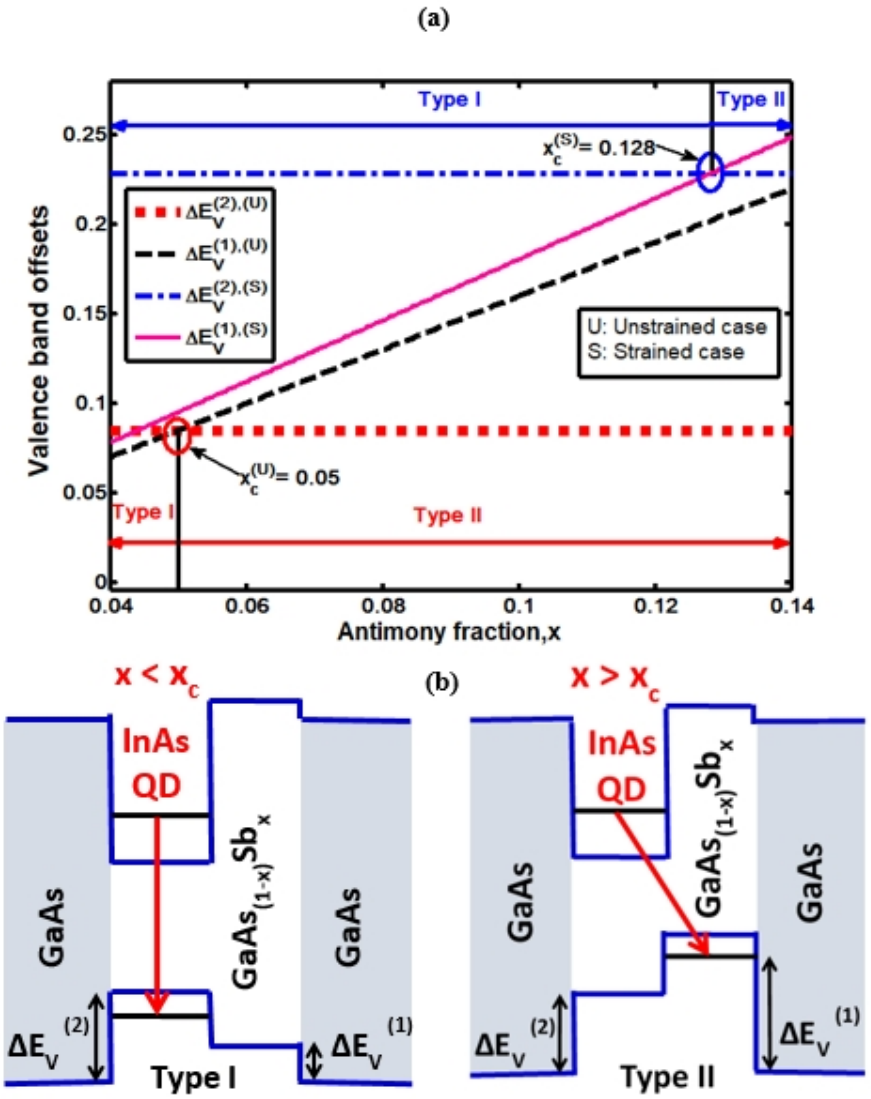

FIG. 2: *(a) Valence band offsets as a function of Sb molar fraction, x, for* $GaAs_{1-x}Sb_x/GaAs$ *interfaces* $\left(\Delta E_V^{(1)}\right)$ *and InAs/GaAs interfaces* $\left(\Delta E_V^{(2)}\right)$*. The superscripts U and S denoted the unstrained and strained case, respectively. The vertical lines represent the critical Sb molar composition for the crossover between* $\Delta E_V^{(1)}$ *and* $\Delta E_V^{(2)}$*. The arrow indicates the transition point. (b) Schematic band diagram of type I and type II transition for* $InAs/GaAs_{1-x}Sb_x/GaAs$ *heterostructure.*

The impact of strain on VB offsets is illustrated in Fig. 2(a), showing the calculated HH band offsets for GaAsSb/GaAs ($\Delta E_V^{(1)}$) and InAs/GaAs ($\Delta E_V^{(2)}$) both in the unstrained and strained cases.

Since the fact that interface (2) is independent of the Sb composition $\Delta E_V^{(2)}$ remains constant for the both cases, while, $\Delta E_V^{(1)}$ is strongly modified by the increase of Sb. We can see that, increasing Sb has a strong impact on the type of the band line-up. When $\Delta E_V^{(1)}$ reaches the $\Delta E_V^{(2)}$ value, $\Delta E_V^{(1)} = \Delta E_V^{(2)}$, the antimony composition achived its critical value indicating a band alignment transition from type I to type II configuration has occurred. This assertion will be discussed and confirmed hereafter. It could be seen that the critical point x_C occurs at $x_C^U = 0.05$ for the unstrained case, and at $x_C^S = 0.128$ in the strained case. To clarify the different optical properties of the investigated structures, a type I/ type II schematic band line-up are represented in Fig 2 (b).

III. EXCITON AND OPTICAL PROPERTIES

In this section, we will check the accuracy of our approach by comparing the theoretical results with experimental data. We first calculated the carrier wave function (WF) distribution of ground state and its localization inside the QD. Second, we evaluated the binding energies to determine the excitonic transition energy, and to understand in more detail the effect of the type-I to type-II transition in the InAs/$GaAs_{1-x}Sb_x$ system. Finally, the carrier lifetimes has been evaluated, and compared to available experimental data.

A. Theoretical model

1. Shape modeling

We start by modeling the QD shape, adopting a realistic representation of its form. A scheme describing the QD shape and their corresponding parameters is given in Fig. 3. The QD shape has been theoretically modeled considering similar initial conditions used in experimental growth procedure proposed by Debnath et *al* [14]. From Atomic Force Microscopy (AFM) images capturing an uncapped InAs QD layer, they scrutinized the surface morphology and dot size. They considered the dots to have a lens-shaped structure with a 0.26 aspect ratio (height/base diameter ratio), while keeping the dot radius fixed at $R = 7.5$ nm. Subsequently, we calculate the single carrier energy levels, E_ν ($\nu =$ e or h), and their correspondant WFs, $\Psi_\nu(r_\nu)$ by combining the realistic description of the QD

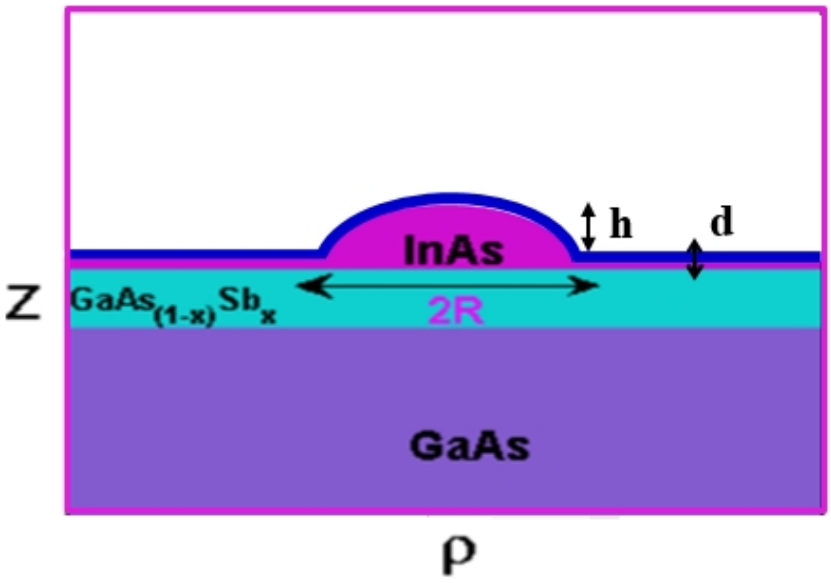

FIG. 3: Schematic model for the lens shape QD structure, R denotes the QD radius, h represents the QD height and d stands for the wetting layer thickness.

shape and the BenDaniel-Duke model [39]. We solve the single-particle Schrödinger equation $H_\nu \Psi_\nu(r_\nu) = E_\nu \Psi_\nu(r_\nu)$, where $H_\nu = T_\nu + V_\nu$, H_ν is the single-particle Hamiltonian, T_ν is the kinetic energy operator of the particle ν, and V_ν is the confinement potential describing the offset between the well material/ barrier material.

2. Coulomb interaction

Having determined $(E_\nu, \Psi_\nu(r_\nu))$, we now turn to calculate the electron-hole Coulomb interaction in both cases, i.e., when considering type-I or type-II QDs.

a. ***Type-I QD:*** In this case, the localizing potential for each carrier is usually much larger than the Coulombic interaction $V^i_{e(h)}$, since, the electron and hole are confined within the dot. Consequently, in the strong confinement regime, the exciton binding energy $\left|V^0_{e(h)}\right|$ can be treated using the perturbative approach. With well-defined distributions of electrons and holes, the direct Coulomb integral can be expressed by the following expression:

$$V^i_{e(h)} = -\frac{e^2}{4\pi\varepsilon_0\varepsilon_r}\int\int \frac{\left|\psi^i_e(\mathbf{r}_e)\right|^2\left|\psi^j_h(\mathbf{r}_h)\right|^2}{|\mathbf{r}_e - \mathbf{r}_h|} d^3\mathbf{r}_e d^3\mathbf{r}_h \tag{9}$$

where ε_r is the dielectric constant inside the QD material, namely InAs in our system. $\psi_e^i(\mathbf{r}_e)$ and $\psi_h^j(\mathbf{r}_h)$ are the electron and hole envelope WFs in the ith and jth energy state, respectively.

The ground state excitonic energy of type I QDs, $E_{exc}^{(I)}$, can be expressed as follows:

$$E_{exc}^{(I)} = E_g^S + E_0^e + E_0^h - \left|V_{e(h)}^0\right| \tag{10}$$

where E_g^S is the bulk band-gap energy of strained InAs. The ground state energies of the electron, E_0^e, and the hole, E_0^h, are calculated with respect to the bottom of CB for E_0^e and the top of VB for E_0^h.

b. ***Type-II QD:*** Due to a situation where the electron and the hole are spatially separated in a type II QD, the treatment and the evaluation of the direct electron-hole interaction in type-II configuration is different from the case corresponding to type I QD. In type II configuration, the hole being localizated outside the QD, their environment is quite different than the electrons which are confined inside the dot. Hence, the electron remains unaffected by the Coulombic interaction, which is two orders of magnitude smaller than the confined potential of the electrons. As for the hole, it experiences both the attractive Coulomb (V_C) due to the confined electrons and the repulsive potential of the dot (V_f), arising from the VB effective barrier. The substantial alteration of the WFs of the carriers outside the QD requires a self-consistent approach for calculating the Coulomb interaction. We follow the procedure detailed in Ref [40] for self-consistent calculations in type II QDs AlInAs/AlGaAs. Indeed, we initiate the calculation of the electron's WF $\left(\psi_e^0\right)$ within the effective mass approximation, disregarding the Coulomb interaction between the electron and the hole. Subsequent step, we will calculate the WF of the hole $\left(\psi_h^0\right)$ by accounting for the contribution of the entire potential $\mathcal{V} = (V_C + V_f)$. Note that only the free hole undergoes the Coulomb potential which is given by:

$$V_C = -\frac{e^2}{4\pi\varepsilon_0\varepsilon_r}\int \frac{\left|\psi_e^0(\mathbf{r}_e)\right|}{|\mathbf{r}_e - \mathbf{r}_h|} d^3\mathbf{r}_e \tag{11}$$

Finally, the ground-state excitonic energy in type- II QD, $E_{exc}^{(II)}$, can be calculated using the following expression:

$$E_{exc}^{(II)} = E_g^B - (\Delta E_C^{(2),(S)} + \Delta E_V^{(2),(S)}) + E_0^e - \mathcal{E}_0^h \tag{12}$$

where E_g^B is the barrier band-gap energy, namely GaAsSb barrier material, $\mathcal{E}_0^h$ is the hole ground-state energy obtained by adopting the self-consistent method which takes into account the spatial separation between carriers, and $\Delta E_C^{(2),(S)}$, $\Delta E_V^{(2),(S)}$ can be calculated following the Eq. (5) and (6), respectively.

3. Radiative exciton lifetime

The probability of the radiative recombination is inversely proportional to the time of the radiative recombination, and it is straightforward related to the QDs absorption cross section. It is thus a fundamental parameter for characterizing and designing optoelectronic applications. The time of the radiative recombination in InAs/GaAsSb QDs can be obtained by using the following expression [41]:

$$\frac{1}{\tau_{rad}} = \frac{4e^2 n E_{exc}}{3m_0^2 c^3 \hbar^2 \pi \epsilon_0} \sum_e |\langle 0| \mathbf{e}.\mathbf{p} |X\rangle|^2$$

where n is the refractive index of the surrounding medium, E_{exc}, is the energy of the exciton optical transition, m_0 is the free-electron mass, c is the light speed in the vaccum; $|0\rangle$ denoted the vaccum state and $|X\rangle$ the exciton state, and $\mathbf{e}$ represents light polarization vector. Using the following relationship: $\sum_e |\langle 0| \mathbf{e}.\mathbf{p} |X\rangle|^2 = \frac{KP^2}{18}$, we finally get

$$\frac{1}{\tau_{rad}} = \frac{1}{137}\frac{4}{9}\frac{n E_{exc} E_p K}{\hbar m_0 c^2} \tag{13}$$

where E_P is the Kane energy defined as $E_P = \frac{2P^2}{m_0}$, P being the interband momentum matrix element, and K is the square of the overlap integral.

We distinguish two exciton regimes to calculate E_{exc} and K. The first regime corresponds to the type I configuration and we adopt the procedure described in subsection 2-a. The second regime describes the type II configuration (see subsection 2-b.).

B. Numerical results and discussions

We will first inspect the WF and for this purpose, the probability densities of the electron ground-state WF, $|\Psi_e|^2$, are shown in Fig. 4(a). It can be clearly noticed that the electron is well-localized inside the QD and it is almost uniformly distributed for $x = 0.07$ (type I QD) and for $x = 0.14$ (type II QD). The contour maps depicted in Fig. 4(b) also indicate

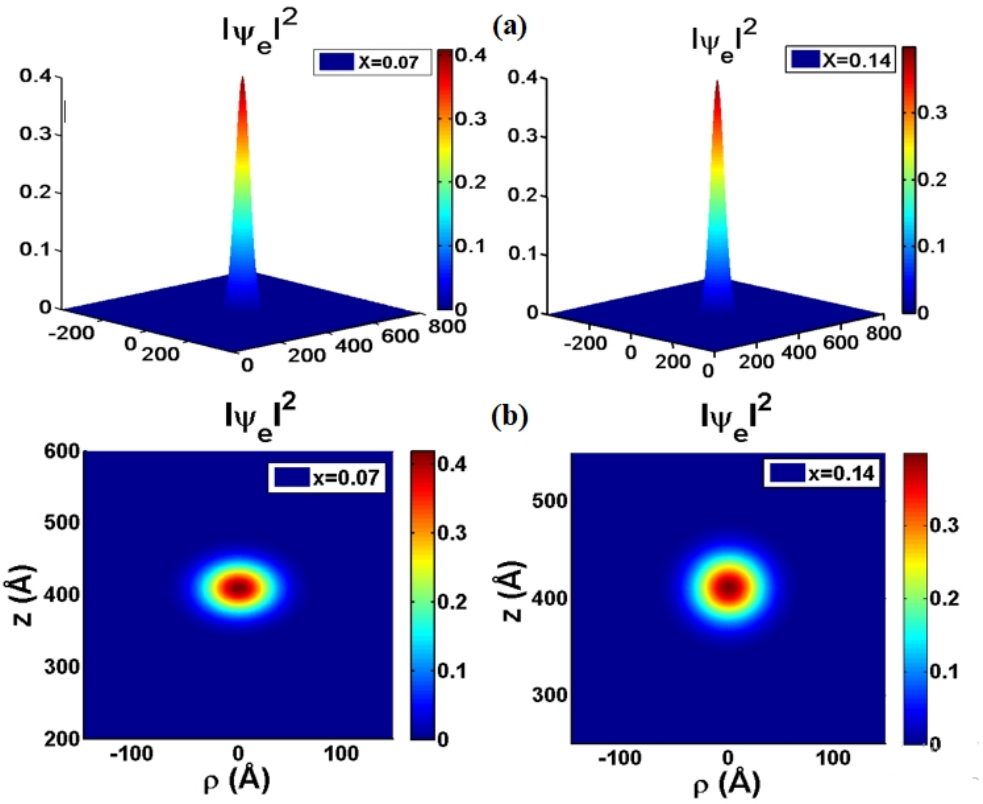

FIG. 4: *(a) Electron probability densities of* $InAs/GaAs_{0.93}Sb_{0.07}$ *type I and* $InAs/GaAs_{0.86}Sb_{0.14}$ *type II QDs with* $R = 7.5$ nm, *and their contour map. (b) Electron contour maps for* $InAs/GaAs_{1-x}Sb_x$ *QDs with different Sb compositions* ($x = 0.07$, $x = 0.14$)

that the electron probability density maxima are minimally influenced by changes in the Sb composition. This implies that the electron WF remains unaffected by variations in the parameter x_{Sb}.

The evolution of ground state hole probability density is depicted in Fig. 5(a). For $x = 0.07$, the holes are predominantly found in the InAs QD, while they are located outside the dot for $x = 0.14$. It should be pointed that for $x = 0.07$, electrons and holes are well localized inside the dot and $|\Psi_h|^2$ is more extended than $|\Psi_e|^2$, indicating that the electrons are more confined in the type I QD than the holes. This behavior is mainly attributed to the difference between the effective masses of the two carriers. Fig. 5(b) shows the contour map for the hole WF of QDs for different Sb compositions. With increasing x, the hole WF is localized in the barrier and close to the QD base. Hence, the WF maximum localization is concentrated above and below the dot, and the $|\Psi_h|^2$ peak shifts gradually further away

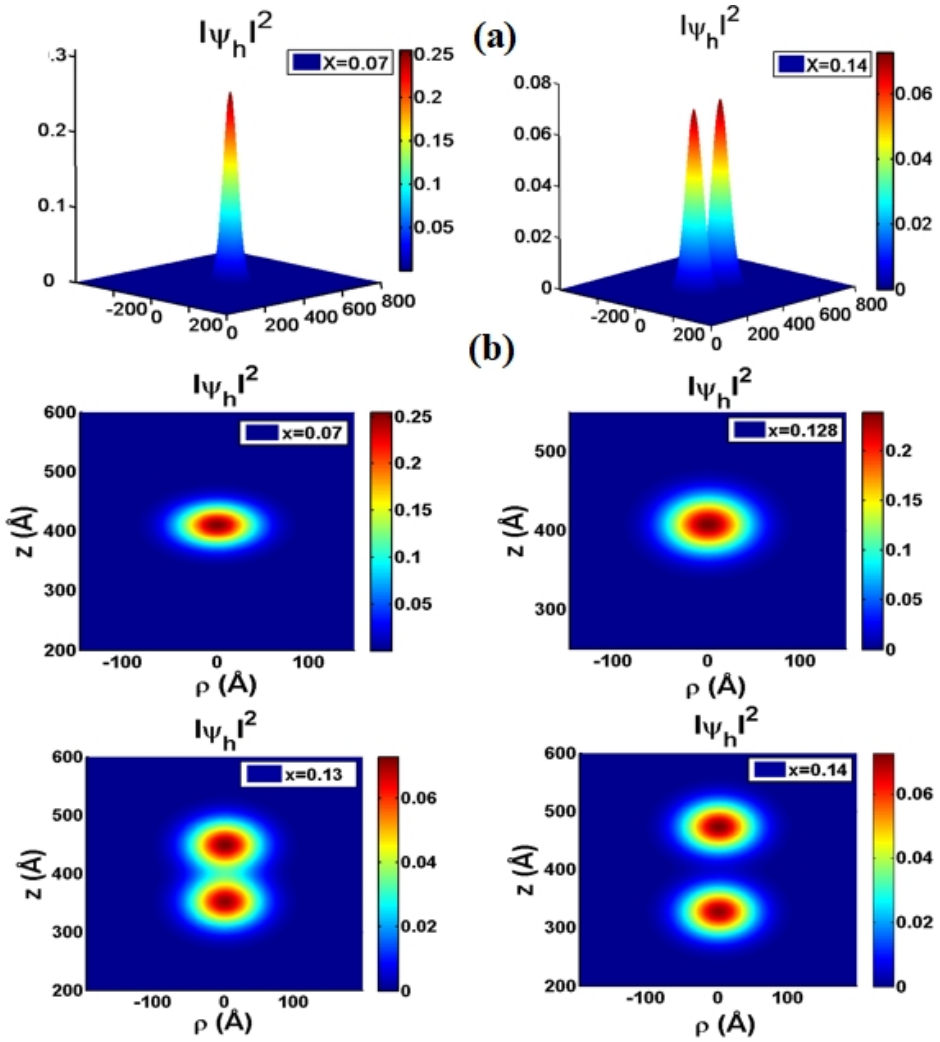

FIG. 5: *(a) Hole probability densities of InAs/GaAs$_{0.93}$Sb$_{0.07}$ type I QD and InAs/GaAs$_{0.86}$Sb$_{0.14}$ type II QD with $R = 7.5$ nm. (b) Hole contour maps for InAs/GaAs$_{1-x}$Sb$_x$ QDs with different Sb molar fractions.*

from the QD. It can be seen that the probability of finding the hole around the lateral walls of the dot is usually slightly small. This means that holes are expelled from the InAs QD and eventually become localized in the GaAs$_{1-x}$Sb$_x$ layer. Consequently, the hole WF does not form a ring around the dot indicating that InAs/GaAs$_{1-x}$Sb$_x$ interface has switched in a type II configuration. In particular, for $x = 0.128$ the maximum of the distribution of the hole WF is split in two parts located outside the dot. This clearly indicates that holes escape to the GaAsSb layer and $x_C = 0.128$ can be defined as a critical point for which the type I - type II transition is likely taking place. The critical Sb composition predicted here

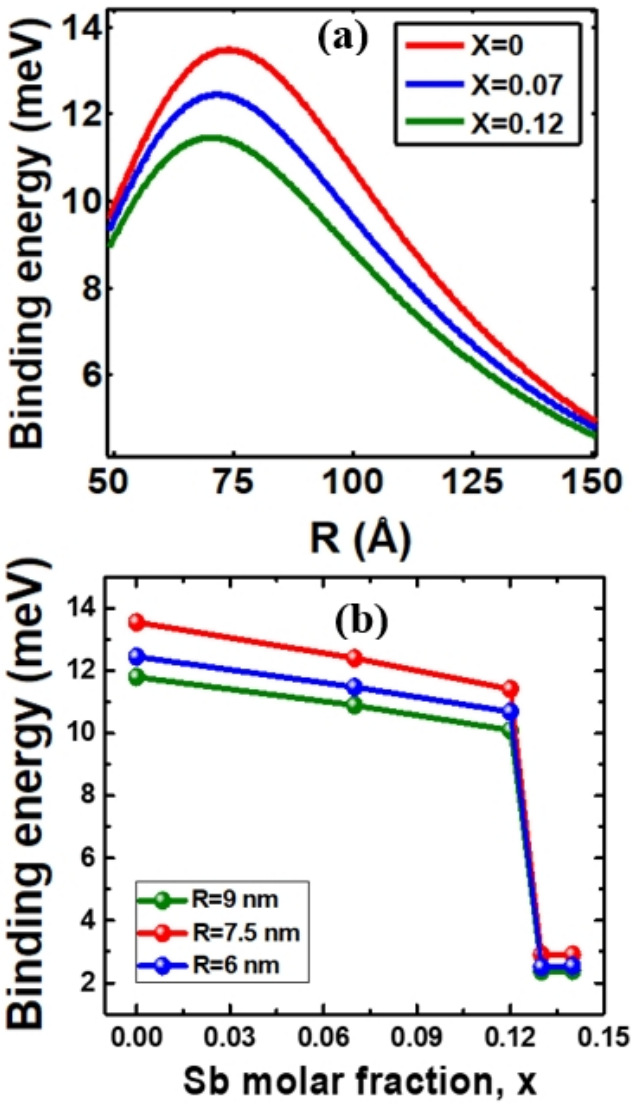

FIG. 6: *(a) The exciton binding energy as a function of QD radius, R, for* $InAs/GaAs_{1-x}Sb_x$ ($x = 0.0$, $x = 0.07$, $x = 0.12$) *type I QDs. (b) The exciton binding energy as a function of Sb composition, x. Three different QDs radii are considered:* $R = 6$ nm, $R = 7.5$ nm, *and* $R = 9$ nm.

agrees very well with the experimental value given in Ref [14] and it is in line with other experimental values [10, 13]. It is clear that the gradual evolution from type I configuration to type II one is closely related to the modification of VB offset due to the increase of antimony atoms in GaAsSb layers, as previously reported in Fig. 2.

After predicting the critical Sb composition for type I-type II transition, we now inves-

tigate the exciton properties and their dependence with the Sb composition and QDs size. For this purpose, we have estimated the exciton binding energy of the ground state for both configurations (I and II). Fig. 6(a) displays the binding energy calculated using Eq. (9) plotted against R, with x values of 0, 0.07, and 0.12. For the same size of QD, the maxima is weaker when the antimony composition is higher, this can be attributed to the decrease of the electron-hole WF overlap. As the QD radius increases from $R = 5$ nm to $R = 15$ nm., the exciton binding energy increases rapidly until it peaks at approximately 14 meV around $R_{\max} \simeq 7.5$ nm. Subsequently, it slowly decreases for larger radii. This increase in binding energy is attributed to confinement effects, the greater the confinement of carriers the closer they are positioned to each other. For $R < R_{\max}$, the reduction in binding energy associated with the decrease in in R can be ascribed to the prolongation of the WFs outside the dot, signifying that the extension of the carriers' WFs starts to spill over into the barrier material. Beyond $R_{\max}$, the binding energy decreases as the QD radius increases. Indeed, the spatial overlap in the charge carriers WFs becomes weaker as the size QD becomes larger, resulting in a significant decreasing the Coulomb interaction. This effect is strongly enhanced by the increase of WFs extension. The competition between both of these effects decreases the Coulomb electron-hole interaction, thereby reducing the confinement of carriers within the dot. This can be understood by a contest between the spatial confinement potential of the barrier material and the kinetic contribution of the carriers. We can state that our results of the present work are consistent with previous studies [40, 42] where the same dependence of the binding energy with respect to the QD size is observed. On the other hand, for the same size of QD, the binding energy value is weaker when the antimony composition is higher. Indeed, the attenuation of the peak maxima with increasing Sb composition is primarily attributed to the disparity in the spreading of the two carriers' WFs. In fact, as we approach the critical composition, the hole wavefunction tends to propagate further towards the barrier material, thus resulting in a decrease in the electron-hole WF overlap.

Figure. 6(b), displays the dependence of the ground state binding energy as a function of the Sb composition, x, for various QD radii $R = 6$, 7.5 and 9 nm. The binding energy is decreasing with increasing the Sb composition, the decrease is about 10 meV. This arises due to the spatial separation of charge carriers in type II systems, and more precisely the spreading disparity of the WF electron and holes. Such depression is also observed in AlInAs/AlGaAs QDs (see Fig. 5 in Ref. [40]). In the previous study [43], the exciton

binding energy was estimated between 26 meV at $x = 0.1$ (type I QD) and 12 meV at $x = 0.22$ (type II QD) within a similar system. This system was based on the eight-band k·p theory and adopted a pyramidal shape of the dot. In return, our numerical results predict values between 14 meV for a type I QD and 4 meV for a type II QD. This slight discrepancy has been attributed to the geometric design and size of the QDs which are different in both approaches.

Another significant parameter to evaluate the transition position is the ground state excitonic energy, E_{exc}, estimated here by Eq. (10) (Eq. (12)) in type-I (type-II) configuration and shown in Fig. 7(a). On one hand, the E_{exc} energy shows a weak dependence on the antimony composition for $x < 0.12$ and $x > 0.13$. On the other hand, E_{exc} is more sensitive to x and drops rapidly when $0.12 < x < 0.13$, indicating that a modification of the configuration (from type I to type II) occurs within this range of Sb composition. We also compare (see Fig. 7(a)) measured exciton transition energy for three different QD series [14, 44, 45] with theoretical values for calculated by means of Eqs. (10 and 12). In type I QDs, i.e. when $x < x_C$, the data of Refs [14, 44] are close to the present theoretical predictions, where the small difference between the experiment and simulation are mainly attributed to the changed size for different QDs. For the type II configuration, we note that our values ($E_{exc}^{(II)}$) are quite similar to the ones suggested by Ref. [45]. However, one observes a experimental overestimation of E_{exc} given by Refs. [14, 44] compared to the reference [45]. We observe that the exciton transition obtained experimentally exhibits a slight dispersion that is never larger than 150 meV. This dispersion may have originated from the growth procedures used by different authors to obtain the final alloy and/or from the methods used to experimentally determine this physical quantity. The differences between theoretical and experimental outcomes may stem from factors not accounted for in our method. These factors, discussed in the literature, include size effects, shape fluctuations, and their implications for quantum confinement, etc

Kane energy is determined by adjusting the band structure and parameters to match those proposed in the literature. The inset in Fig. 6(b) shows the calculated values of the Kane energy as a function of x. A good understanding of these parameters is essential to optimize and control the optical properties, such as the radiative recombination, of these nanostructure. Thus, the evolution of the radiative lifetime τ_{rad} as a function of Sb composition in InAs/GaAsSb QDs was addressed. In Fig. 6(b), we compare the estimated τ_{rad}

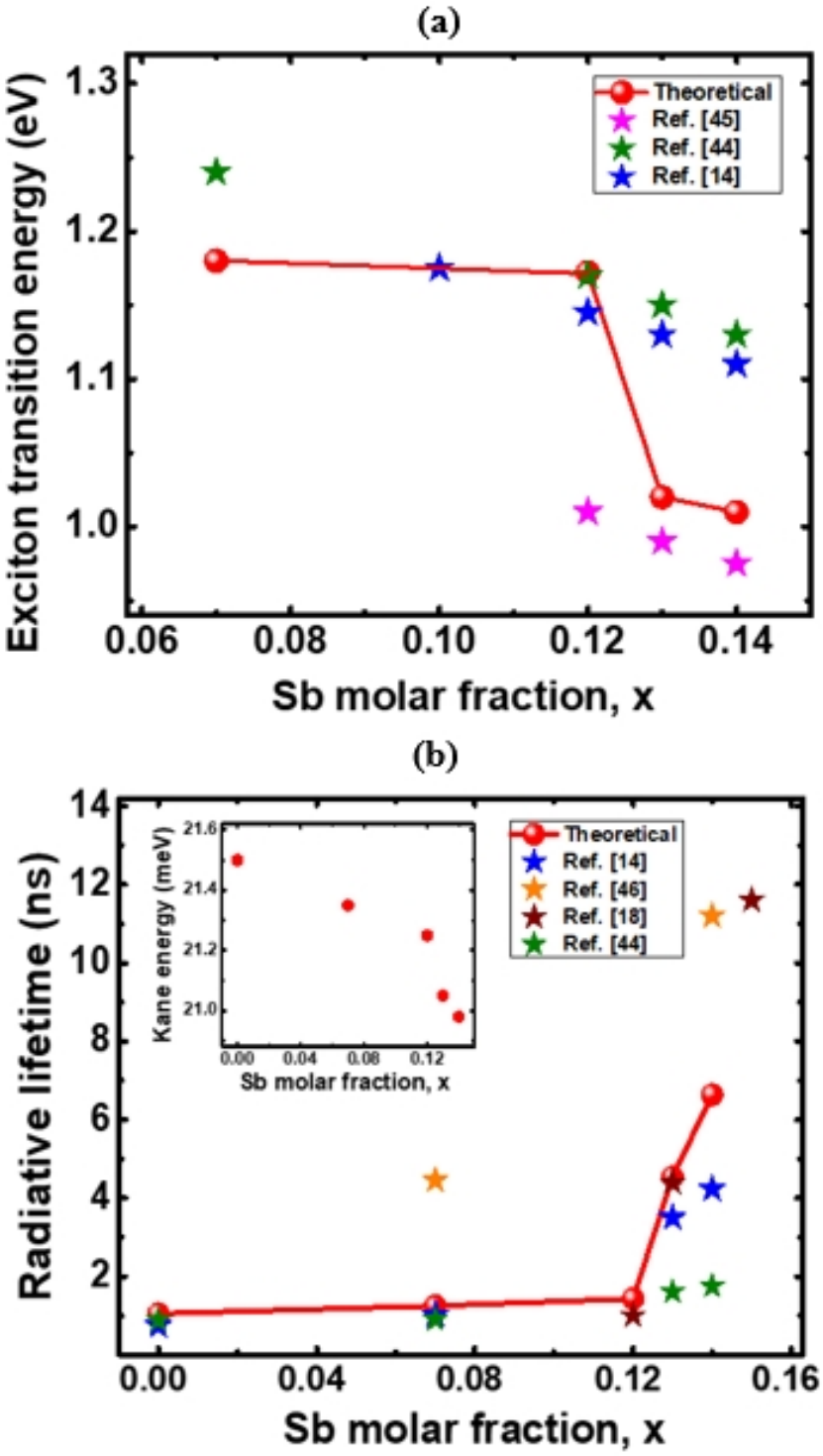

FIG. 7: *a) Calculated (red curve) and measured excitonic transition energy of the ground state as a function of the Sb composition, x. (b) Calculated (red curve) and measured carrier lifetime, τ_{rad}, of $InAs/GaAs_{1-x}Sb_x$* QDs with different Sb compositions ($x = 0.0$, $x = 0.07$, $x = 0.13$, $x = 0.14$). *The inset in (b) shows the Kane energy as a function of the Sb composition.*

with the experimental results [14, 18, 44]. Our calculations predict a lifetime of about 1 ns for type I QDs, this value increases from 4 to 8 ns for type II QDs. It can be seen that our theoretical results show good agreement with the reported experimental data [14, 18]. We note that our values are close to other experimental results have been obtained for an InAs/GaAs/GaAsSb QD system [44], but are shorter than the ones evaluated in Ref. [46]. However, the calculated τ_{rad} much lower than the previously reported values: 24-29 ns for the 16%-21% Sb [47], 65 ns for 22% Sb [48], and 10-20 ns for 16% Sb [49]. This variation may stem from the experimental uncertainties to measure this physical quantity in similar systems. It can be clearly noticed that the increase of τ_{rad} is attributed to the strong delocalisation of hole, as x increases, which causes the reduce of overlap of electron and hole wave functions. For a type-II system, the spatial separation of the electrons and holes in InAs/GaAsSb QDs induces in a much longer lifetime, since, τ_{rad} is inversely proportional to the square of the overlap integral Eq (19). Finally, it can be clearly observed from the current results that carrier lifetime of a type II structure is much longer than that of type I structure which has a greater WF overlapping because the electrons and holes are spatially localized.

IV. CONCLUSION

We have investigated the crossover from type I to type II band line-up of InAs QDs by varying the Sb molar composition in $GaAs_{1-x}Sb_x$ matrix. We found that the electronic structure depends sensitively on the details of QD sructure, and type I - type II transition takes place as the Sb concentration, x, approaches the critical point $x_c = 0.128$. The molar dependence of confined state energy levels and electron/hole WF, and the size dependence of the binding energy have been calculated. The significant depression of the binding energy indicates a type II band alignment for QD structures with $x \geqslant x_C$. The relevance of our approach has been demonstrated by comparing them with the available experimental results. We found that theoretical calculations of optical transition energies have shown a good agreement with experimental findings for type II QDs, while small discrepancies were observed for the type I QDs. Our approach reveals that the calculation of the carrier lifetime ranging from 1 to 10 ns, when the optical transitions changes from direct to indirect. The trend of increasing lifetime with increasing x has been in quantitative agreement with

available experimental data.

---

[1] M. Geller, C. Kapteyn, L. Müller-Kirsch, R. Heitz, and D. Bimberg, Phys. Status Solidi B **238**, 258 (2003).

[2] A. Marent, M. Geller, A. Schliwa, D. Feise, K. Pötschke, D. Bimberg, N. Akçay, and N. Öncan, Appl. Phys. Lett. **91**, 242109 (2007).

[3] R. B. Laghumavarapu, A. Moscho, A. Khoshakhlagh, M. El-Emawy, L. F. Lester, and D. L. Huffaker, Appl. Phys. Lett. **90**, 173125 (2007).

[4] J. Tatebayashi, A. Khoshakhlagh, S. H. Huang, G. Balakrishman, L. R. Dawson, D. L. Huffaker, D. A. Bussian, H. Htoon, and V. Klimov, Appl. Phys. Lett. **90**, 261115 (2007).

[5] K. A. Sablon, J. W. Little, V. Mitin, A. Sergeev, N. Vagidov, and K. Reinhardt, Nano Lett. **11**, 2311 (2011).

[6] T. Li, R. E. Bartolo, and M. Dagenais, Appl. Phys. Lett. **103**, 141113 (2013).

[7] Y. Shoji, K. Akimoto, and Y. Okada, J. Phys. D: Appl. Phys. **46**, 024002 (2013).

[8] P. Lam, J. Wu, L. Tang, Q. Jiang, S. Hatch, R. Beanland, J. Wilson, R. Allison, and H. Liu, Sol. Energy Mater. Sol. Cells **126**, 83 (2014).

[9] A. Kechiantz, A. Afanasev, J.-L. Lazzari, A. Bhouri, Y. Cuminal, and P. Christol, Proceedings of the 27th European Photovoltaic Solar Energy Conference and Exhibition, Frankfurt, Germany, 24-28 September, 2012.

[10] K. -Y. Ban, S. P. Bremner, G. Liu, S. N. Dahal, P. C. Dippo, A. G. Norman, and C. B. Honsberg, Appl. Phys. Lett. **96**, 183101 (2010).

[11] M. Y. Levy and S. Honsberg, IEEE Trans. Electron Devices **55**, 706 (2008).

[12] H. Y. Liu, M. J. Steer, T. J. Badock, D. J. Mowbray, M. S. Skolnick, P. Navaretti, K. M. Groom, M. Hopkinson, and R. A. Hogg, Appl. Phys. Lett. **86**, 143108 (2005).

[13] S. Hatch, J. Wu, K. sablon, P. Lam, M. C. Tang, Q. Jiang, and H. Y. Liu, Opt. Express **22**, A 679 (2014).

[14] M. C. Debnath, T. D. Mishima, M. B. Santos, Y. Cheng, V. R. Whiteside, I. R. Sellers, K.

Hossain, R. B. Laghumavarapu, B. L. Liang, and D. L. Huffaker, J. Appl. Phys. **119**, 114301 (2016).

[15] K. Nishikawa, Y. Takeda, K.-I, Yamanaka, T. Motohiro, D. Sato, J. Ota, N. Miyashita, and Y. Okada, J. Appl. Phys. **111**, 044325 (2012).

[16] H. Y. Liu, M. J. Steer, T. J. Badock, D. J. Mowbray, M. S. Skolnick, F. Suarez, J. S. Ng, M. Hopkinson, and J. P. R. David, J. Appl. Phys. **99**, 046104 (2006).

[17] C. Y. Jin, H. Y. Liu, S. Y. Zhang, Q. Jiang, S. L. Liew, M. Hopkinson, T. J. Badock, E. Nabavi, and D. J. Mowbray, Appl. Phys. Lett. **91**, 021102 (2007).

[18] K. -Y. Ban, D. Kuciauskas, S. P. Bremner, and C. B. Honsberg, J. Appl. Phys. **111**, 104302 (2012).

[19] I. Saïdi, S. Ben Radhia, and K. Boujdaria, J. Appl. Phys. **107**, 043701 (2010).

[20] R. Neffati, I. Saïdi, and K. Boujdaria, J. Appl. Phys. **112**, 053716 (2012).

[21] G. Pikus and G. Bir, Tverd. Tela (Leningrad) 1, 1642 (1960).

[22] S. P. Bremner, K.Y. Ban, N. N. Faleev, C. B. Honsberg and D. J. Smith, J. Appl. Phys. **114**, 103511 (2013).

[23] P. Harrison 2005 *Quantum wells, Wires and Dots: Theoretical and Computational Physics of Semiconductor Nanostructures* (New York, Wiley).

[24] Y. G. Sadofyev and N. Samal, Materials. **3**, 1497 (2010).

[25] I. Vurgaftmana and J. R. Meyer, J. Appl. Phys. **89**, 11 (2001).

[26] A. D. Prins, D. J. Dunstan, J. D. Lambkin, E. P. O'Reilly, A. R. Adams, R. Pritchard, W. S. Truscott, and K. E. Singer, Phys. Rev. B **47**, 2191(1993).

[27] R. Teissier, D. Sicault, J. C. Harmand, G. Ungaro, G. Le Roux, and L. Largeau, J. Appl. Phys. **89**, 5473 (2001).

[28] M. Dinu, J. E. Cunningham, F. Quochi, and J. Shah, J. Appl. Phys. **94**, 1506 (2003).

[29] G. Ji, S. Agarwala, D. Huang, J. Chyi, and H. Morkoc, Phys. Rev. B **38**, 10 571 (1988).

[30] M. Peter, K. Winkler, M. Maier, H. Herres, J. Wagner, D. Fekete, K. H. Bahem, and D. Richards, Appl. Phys. Lett. **67**, 2639 (1995).

[31] G. Liu, S. L. Chang, and F. -Y. Park, J. Appl. Phys. **88**, 5554 (2000).

[32] S. M. North, P. R. Briddon, M. A. Cusack, and M. Jaros, Phys. Rev. B **58**, 12601 (1998).

[33] M. E. Rubin, H. R. Blank, M. A. Chin, H. Kroemer, and V. Narayanamurti, Appl. Phys. Lett. **70**, 1590 (1997).

[34] Pryor. Phys. Rev. B **60**, 2869 (1999).

[35] A. Schliwa, M. Winkelnkemper, and D. Bimberg. Phys. Rev. B **76**, 205324 (2007).

[36] O. L. Lazarenkova, P. V. Allmen, F. Oyafuso, and S. Lee. Appl. Phys. Lett. **85**, 4193 (2004).

[37] R. Colombelli, V. Piazza, A. Badolato, M. Lazzarino, and F. Beltram. Appl. Phys. Lett. **76**, 1146 (2000).

[38] A. Taguchi and T. Ohno, Phys. Rev. B **48**, 17607 (1993).

[39] B. J. BenDaniel and C. B. Duke, Phys. Rev. 152, 683 (1966).

[40] R. Neffati, I. Saïdi, S. Ben Radhia, K. Boujdaria, and C. Testelin, Semicond. Sci. Technol. **30**, 085008 (2015).

[41] Al. L. Efros, Phys. Rev. B **46**, 7448 (1992).

[42] K. L. Janssens, F. M. Peters, and V. A. Schweigert, Phys. Rev. B **63**, 205311 (2001).

[43] P. Klenovsky, V. Krapek, D. Munzar, and J. Humlicek, Appl. Phys. Lett. **97**, 203107 (2010)

[44] A.D. Utrilla, D.F. Reyes, J.M. Llorens, I. Artacho, T. Ben, D. González, Ž. Gačević, A. Kurtz, A. Guzman, A. Hierro and J.M. Ulloa, Solar Energy Materials & Solar Cells. **159**, 282 (2017).

[45] K. Alshehri, A. Salhi, N. Ahamad Madhar and B. Ilahi. Crystals , **9**, 530 (2019).

[46] W. Liu, Y. T. Wang, C.M. Chang, W. Y. Qiu and C. Fang. Phys. Status Solidi C **10**, 1489–1491 (2013).

[47] W. H. Chang, Y. Liao, W. Hsu, M. C. lee, P. C. Chiu, and J. L. Chyi, Appl. Phys. Lett. **93**, 033107 (2008).

[48] Y. D. Jang, T. J. Badcock, D. J. Mowbray, M. S. Skolnick, J. Park, D. Lee, H. Y. Liu, M. J. Steer, and M. Hopkinson, Appl. Phys. Lett. **92**, 251905 (2008).

[49] Y. A. Liao, W. T. Hsu, P. C. Chiu, J. L. Chyi, and W. H. Chang, Appl. Phys. Lett. **94**, 053101 (2009).